ACCEPTED IN APJ
Preprint typeset using LaTeX style emulateapj v. 11/26/03

GRAVITATIONAL LENSING MAGNIFICATION WITHOUT MULTIPLE IMAGING

CHARLES R. KEETON[1,2,3], MICHAEL KUHLEN[4], & ZOLTÁN HAIMAN[5]

Accepted in ApJ

ABSTRACT

Gravitational lensing can amplify the apparent brightness of distant sources. Images that are highly magnified are often part of multiply-imaged systems, but we consider the possibility of having large magnifications without additional detectable images. In rare but non-negligible situations, lensing can produce a singly highly magnified image; this phenomenon is mainly associated with massive cluster-scale halos ($\gtrsim 10^{13.5}\,M_\odot$). Alternatively, lensing can produce multiply-imaged systems in which the extra images are either unresolved or too faint to be detectable. This phenomenon is dominated by galaxies and lower-mass halos ($\lesssim 10^{12}\,M_\odot$), and is very sensitive to the inner density profile of the halos. Although we study the general problem, we customize our calculations to four quasars at redshift $z \approx 6$ in the Sloan Digital Sky Survey (SDSS), for which Richards et al. (2004) have ruled out the presence of extra images down to an image splitting of $\Delta\theta = 0\farcs3$ and a flux ratio of $f = 0.01$. We predict that 9–29% of all $z \approx 6$ quasars that are magnified by a factor of $\mu > 10$ would lack detectable extra images, with 5–10% being true singly-imaged systems. The maximum of 29% is reached only in the unlikely event that all low-mass ($\lesssim 10^{10}\,M_\odot$) halos have highly concentrated (isothermal) profiles. In more realistic models where dwarf halos have flatter (NFW) inner profiles, the maximum probability is $\sim 10\%$. We conclude that the probability that *all four* SDSS quasars are magnified by a factor of 10 is $\lesssim 10^{-4}$. The only escape from this conclusion is if there are many (>10) multiply-imaged $z \approx 6$ quasars in the SDSS database that have not yet been identified, which seems unlikely. In other words, lensing cannot explain the brightnesses of the $z \approx 6$ quasars, and models that invoke lensing to avoid having billion-$M_\odot$ black holes in the young universe are not viable.

Subject headings: gravitational lensing — cosmology: theory — quasars: general

1. INTRODUCTION

Two conspicuous aspects of gravitational lensing are the ability to (i) produce multiple images, and (ii) magnify the apparent brightness of a distant background source. Large magnifications generally require that the projected density along the line of sight be of order the critical surface density for lensing, which in turn implies a precise alignment of the observer, the lens, and the source. The same condition generally leads to the production of multiple images, so in most cases one expects highly magnified objects to have at least one companion lensed image.

The connection between magnification and multiple imaging can be important in a variety of contexts. An important example, which serves as the main motivation for this paper, is the recent discovery of bright quasars at redshifts as high as $z \sim 6$ in the Sloan Digital Sky Survey (SDSS; see Fan et al. 2000, 2001, 2003). If these quasars are not lensed or beamed (see Haiman & Cen 2002 and Willott, McLure, & Jarvis 2003 for arguments to justify both assumptions), they are inferred to be very luminous ($M_B \sim -27$). Assuming further that they shine at the Eddington limit of their resident black holes (BH), these BHs must have masses of several $\times 10^9\,M_\odot$.

Having such massive BHs at such an early stage in the evolution of the universe presents a challenge to models where massive BHs grow mainly by gas accretion that is itself Eddington limited (Haiman & Loeb 2001). Even in the context of hierarchical structure formation models, where mergers of several BHs can contribute to the build-up of the mass, the initial seeds are required to be present as early as $z \gtrsim 15$ (Haiman & Loeb 2001). The problem is exacerbated if BH–BH mergers result in the ejection of BHs from the shallow dark matter potential wells at high redshift because of a large recoil following the emission of gravitational waves. In a recent model that includes this effect, Haiman (2004) found that BHs can grow by mergers and accretion to at most a few $\times 10^8$ M$_\odot$ by redshift $z = 6.4$ without a super-Eddington phase — a short-fall by a factor of ~ 10 relative to the BH masses inferred from observations.

If the high-redshift quasars were magnified by gravitational lensing by a factor of $\mu \gtrsim 10$, this could alleviate the need for a super-Eddington growth phase to explain such massive early BHs (since the inferred mass scales as μ^{-1} under the assumption that the quasar is shining at the Eddington luminosity). Although the lensing optical depth along a random line of sight to $z \sim 6$ is known to be small ($\sim 10^{-3}$; e.g., Kochanek 1998; Barkana & Loeb 2000), magnification bias can significantly boost the probability of strong lensing in a real, flux-limited survey. If the intrinsic (unlensed) quasar luminosity function at $z \sim 6$ is steep, and/or it extends to faint magnitudes, the probability of strong lensing for the SDSS quasars could even be of order unity (Comerford et al. 2002; Wyithe & Loeb 2002). However, for a population of isothermal sphere lenses, all magnifications $\mu > 2$ are associated with multiple imaging, and in most cases the angular separation between the images is more than $0\farcs3$ (Comerford et al. 2002). Recent HST observations of the highest redshift quasars have shown no evidence for additional images of any of the $z \approx 6$ sources down to a splitting angle of $0\farcs3$ (Richards et al. 2004), which effectively rules out the hypoth-

[1] Astronomy & Astrophysics Department, University of Chicago, 5640 S. Ellis Ave., Chicago, IL 60637
[2] Hubble Fellow
[3] Department of Physics & Astronomy, Rutgers University, 136 Frelinghuysen Road, Piscataway, NJ 08854
[4] Department of Astronomy & Astrophysics, University of California, 1156 High St., Santa Cruz, CA 95064
[5] Department of Astronomy, Columbia University, 550 W. 120th St., New York, NY 10027

esis that the quasars are all highly magnified by *isothermal sphere* lenses.

The obvious question is whether the SDSS quasars could be magnified by lenses with a more complicated (and indeed more realistic) lens potential, without producing multiple detectable images. Wyithe & Loeb (2002) showed that microlensing by stars within lens galaxies can permit magnifications as high as $\mu \sim 10$ for singly-imaged quasars, but the probability for $\mu > 2$ is still very low (<0.5% even when magnification bias is included). Another question is whether departures from spherical symmetry significantly affect the results. One goal of this paper is to study ellipticity in the lens galaxy and tidal shear from objects along the line of sight, both of which are common in observed multiply-imaged systems (e.g., Keeton, Kochanek, & Seljak 1997; Witt & Mao 1997; Holder & Schechter 2003). Ellipticity and shear are known to modify the full magnification distribution for multiply-imaged sources (e.g., Blandford & Kochanek 1987; Finch et al. 2002; Huterer et al. 2004); but what happens when we restrict attention to sources without multiple detectable images is not known. More generally, our goal is to present a thorough and general study of the magnifications that can be produced by lenses with different radial profiles and angular shapes, without creating multiple detectable images. We simultaneously consider both true singly-imaged systems, as well as multiply-imaged configurations where the images are too close to be resolved or the extra images are below some reasonable detection threshold.

In this thorough but technical study, let us not lose sight of the bottom line: We find that the *maximum* probability that a $z \approx 6$ quasar is magnified by at least a factor of 10 without having a second detectable image is 29% (see Table 1). Moreover, this maximum is reached only in the unlikely event that halos down to arbitrarily low mass have highly concentrated (singular isothermal sphere) profiles. In more realistic models of the lensing population, where dwarf halos have flatter (NFW) inner profiles, the maximum probability is $\sim 10\%$.

While our analysis is specifically prompted by the SDSS quasars, it should be applicable to other objects for which significant lensing amplification would be important, such as high-redshift galaxies discovered in "blank" fields[6] (i.e., fields not specifically chosen for the presence of a massive cluster lens;e.g., Rhoads et al. 2000; Rhoads & Malhotra 2001; Steidel et al. 2003; Bouwens et al. 2003; Ouchi et al. 2003; Stanway et al. 2004; Pirzkal et al. 2004).

This paper is organized as follows. In § 2, we review the relevant lens theory and summarize our calculation methods. In the technical core of the paper (§§ 3-4), we study the magnification properties of simple but useful lens potentials: ellipsoidal isothermal and NFW halos, with external tidal shear. The idea is to identify general features and understand the parameter dependences. Building on this foundation, in § 5 we compute the probability of magnification without multiple imaging for a realistic lens population, and discuss the implications for the SDSS quasars. Finally, in § 6 we summarize our results. Throughout the paper, we assume a ΛCDM cosmology with $\Omega_M = 0.3$, $\Omega_\Lambda = 0.7$, $\sigma_8 = 0.9$, and $H_0 = 70$ km/s/Mpc, consistent with the recent results from WMAP (Spergel et al. 2003).

[6] Magnification of high-redshift sources by foreground cluster lenses is certainly interesting and important (e.g., Hu et al. 2002; Kneib et al. 2004; Pelló et al. 2004). However, deliberate selection of cluster fields makes the probability analysis completely different from what we study here.

2. COMPUTATION METHODS

The lensing properties of a system can be derived from the lens potential ϕ, which is given by the solution to the 2-d Poisson equation $\nabla^2\phi = 2\kappa$. Here $\kappa = \Sigma/\Sigma_{\rm crit}$ is the surface mass density in units of the critical density for lensing, $\Sigma_{\rm crit} = (c^2 D_{os})/(4\pi G D_{ol} D_{ls})$, where D_{ol}, D_{os}, and D_{ls} are angular diameter distances between the observer, lens, and source. (See Schneider, Ehlers, & Falco 1992 for a full discussion of lens theory.) The relation between the position $\mathbf{x}$ of an image and the position $\mathbf{u}$ of the corresponding source is given by the lens equation,

$$\mathbf{u} = \mathbf{x} - \nabla\phi(\mathbf{x}) . \tag{1}$$

The magnification of an image at position $\mathbf{x}$ is

$$\mu(\mathbf{x}) = \left| \begin{array}{cc} 1 - \frac{\partial^2\phi}{\partial x^2} & -\frac{\partial^2\phi}{\partial x \partial y} \\ -\frac{\partial^2\phi}{\partial x \partial y} & 1 - \frac{\partial^2\phi}{\partial y^2} \end{array} \right|^{-1} \tag{2}$$

The lensing critical curves are curves in the image plane where the magnification is formally infinite, and the caustics are the corresponding curves in the source plane. Sources that lie outside the caustics are singly imaged, while sources inside the caustics have multiple images. We use the *gravlens* software by Keeton (2001a) to find the caustics, solve the lens equation, and compute the image magnifications for the various models we consider.

We are interested in the cross section for having a magnification (of a single image, or a combination of unresolved images) larger than μ, which we compute with Monte Carlo simulations. For singly-imaged sources, we set a minimum magnification $\mu_{\rm min}$ of interest, typically $\mu_{\rm min} = 1.5$, and find the smallest circle in the image plane such that all images outside the circle have $\mu < \mu_{\rm min}$; this ensures that all of the images of interest lie inside the circle. We then pick $\sim 10^6$ random image positions in the circle. The cross section for producing a singly-imaged system with magnification greater than μ can be written as

$$A_{\rm sing}(\mu) = \int_{\mu(\mathbf{u})>\mu} d\mathbf{u} = \int_{\mu(\mathbf{x})>\mu} \frac{1}{\mu(\mathbf{x})}\, d\mathbf{x} . \tag{3}$$

The first integral is over all source positions $\mathbf{u}$ where there is only one image and it has magnification greater than μ. The second integral is over the corresponding image positions, and the equality holds because $\mu^{-1} = |\partial\mathbf{u}/\partial\mathbf{x}|$ is the Jacobian of the transformation between the image and source planes. In other words, the cumulative singly-imaged magnification distribution can be computed by simply summing the images, weighted by their inverse magnifications.

For multiply-imaged sources, we find the smallest circle enclosing the caustics, then pick $\sim 10^6$ random sources in this circle and solve the lens equation to find the image configurations. Now we throw away the singly-imaged systems, and use the multiply-imaged systems to compute the cross section for having a magnification greater than μ but no extra *detectable* images,

$$A_{\rm mult}(\mu) = \int_{\mu(\mathbf{u})>\mu} S(\mathbf{u})\, d\mathbf{u} . \tag{4}$$

This integral spans the multiply-imaged region, but the function $S(\mathbf{u})$ selects source positions that produce lenses with only a single detectable image; specifically, $S(\mathbf{u})$ is 1 if the additional images are undetectable (either because they are

too faint, or too close to the brightest image), and 0 otherwise. In general, $S(\mathbf{u})$ will depend on the specific source, instrument, and observational conditions. Hereafter we refer to it as the "single-detectable-image criterion" (SDIC). In recent HST images of the $z \approx 6$ SDSS quasars, Richards et al. (2004) were able to rule out the presence of extra images with a flux ratio relative to the quasar of $f > 0.01$ down to a separation $\Delta\theta > 0\farcs3$, or brighter than $f > 0.1$ down to $\Delta\theta > 0\farcs1$. We consider both of these SDICs in our analysis. In configurations where there are multiple images that would not be resolved, we include all of them in the net magnification.

3. ISOTHERMAL HALOS

The isothermal ellipsoid is a simple but surprisingly useful model for studying lensing by galaxies. In this section we delineate the situations in which isothermal halos can produce magnification without detectable multiple images.

3.1. *Definitions of Ellipticity and Shear*

Early-type galaxies, which dominate the lensing optical depth at image separations $\Delta\theta \lesssim 4''$, appear to have nearly-isothermal profiles based on evidence from strong and weak lensing, stellar dynamics, satellite kinematics, and X-ray studies (e.g., Fabbiano 1989; Zaritsky & White 1994; Rix et al. 1997; Gerhard et al. 2001; McKay et al. 2002; Treu & Koopmans 2002; Koopmans et al. 2003; Rusin et al. 2003b; Sheldon et al. 2004). The 3-d density $\rho \propto r^{-2}$ and projected surface mass density $\kappa \propto R^{-1}$ correspond to a flat rotation curve or velocity dispersion profile, and a deflection angle that is independent of impact parameter.

The lensing properties of a *singular isothermal sphere* are very simple (e.g., Schneider et al. 1992). The surface mass density is $\kappa = R_{\rm ein}/(2R)$ where $R_{\rm ein}$ is the Einstein radius, and the lensing potential is $\phi = R_{\rm ein} R$. A source at radius $u > R_{\rm ein}$ behind the lens produces a single image at radius $R = R_{\rm ein} + u$ which has magnification $\mu = R/(R - R_{\rm ein}) = 1 + R_{\rm ein}/u$. A source at radius $u < R_{\rm ein}$ produces two images at radii $R_\pm = R_{\rm ein} \pm u$ on opposite sides of the lens galaxy, which have magnifications $\mu_\pm = R_\pm/(R_\pm - R_{\rm ein}) = 1 \pm R_{\rm ein}/u$ (where a negative magnification means that the image is parity reversed).

An *isothermal ellipsoid* has a projected surface mass density of

$$\kappa(R,\theta) = \frac{b}{2R}\left[\frac{1+q^2}{(1+q^2)-(1-q^2)\cos 2\theta}\right]^{1/2}, \qquad (5)$$

where $q \leq 1$ is the axis ratio, so the ellipticity is $e = 1-q$, and (R,θ) are polar coordinates centered on the lens galaxy. (Without loss of generality, we are working in coordinates aligned with the major axis of the galaxy.) The lensing properties of an isothermal ellipsoid are given by Kassiola & Kovner (1993), Kormann, Schneider, & Bartelmann (1994), and Keeton & Kochanek (1998). For a spherical galaxy the parameter b equals the Einstein radius, while for a nonspherical galaxy we can relate them by (see Huterer et al. 2004)

$$\frac{R_{\rm ein}}{b} = \frac{1}{\pi}\left[2(1+q^{-2})\right]^{1/2} K\left(1+q^{-2}\right), \qquad (6)$$

where $K(x)$ is the elliptic integral of the first kind.

Gravitational tidal shear, produced by objects near the main lens halo or projected along the line of sight, can increase the probability for high magnifications. Shear is expected to be common, based on both analytic estimates and numerical simulations (e.g., Keeton et al. 1997; Holder & Schechter 2003), and it is generally required for fitting observed galaxy-mass ($M \sim 10^{12} M_\odot$) strong lens systems (e.g., Keeton et al. 1997; Witt & Mao 1997). The lens potential associated with shear is

$$\phi(R,\theta) = -\frac{1}{2}R^2\gamma\cos 2(\theta-\theta_\gamma), \qquad (7)$$

where γ is the dimensionless shear amplitude, θ_γ is the shear direction. Shears of $\gamma \sim 0.05$–0.1 are common for galaxy-mass lenses, and shears of $\gamma \sim 0.2$–0.3 are possible for lens galaxies lying in dense environments (e.g., Keeton et al. 1997; Witt & Mao 1997; Kundić et al. 1997a,b; Fischer et al. 1998; Kneib et al. 2000; Holder & Schechter 2003).

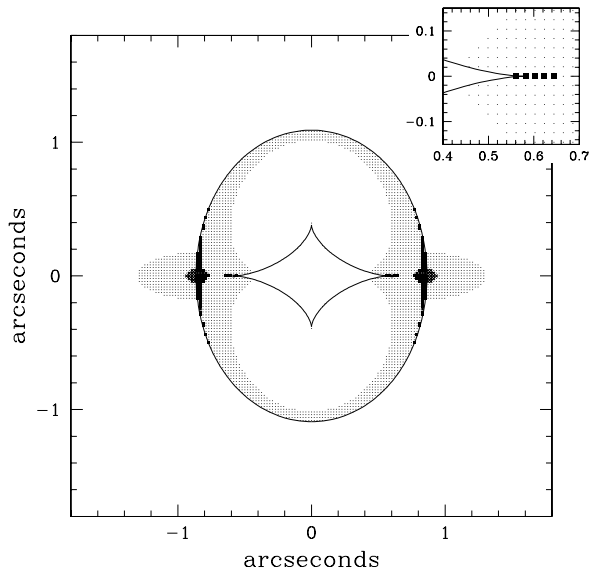

FIG. 1.— Source plane for an isothermal ellipsoid with ellipticity $e = 0.5$ and Einstein radius $R_{\rm ein} = 1\farcs0$. The curves show the caustics. The small (large) points outside the caustics indicate singly-imaged sources with magnification $\mu > 3$ ($\mu > 5$). The points inside the caustic show multiply-imaged sources for which extra images are undetectable; the small (large) points denote a flux ratio threshold $f < 0.1$ ($f < 0.01$). The inset shows a close-up of the tip of the inner caustic.

3.2. *Parameter Dependences for a Single Lens*

To begin to understand isothermal lenses, we show the source plane for a sample lens with ellipticity $e = 0.5$ in Figure 1. Singly-imaged sources with magnification $\mu > 3$ occur only in a region just outside the caustics and near the minor axis of the radial caustic (which corresponds to the major axis of the galaxy density distribution). In this example with Einstein radius $R_{\rm ein} = 1''$, the image separations are larger than HST resolution, so the only systems that have only one detectable image are those whose extra images are too faint. Most of these are small flux ratio doubles, corresponding to sources that lie in two regions: just inside the outer radial caustic, where the secondary image is very faint; or near the inner tangential caustic, especially near the cusps along the major axis, where the primary image is highly magnified. In this example the two regions merge together when the flux ratio threshold for missing the second image is $f < 0.1$ (the small points in Figure 1), but remain distinct when the threshold is $f < 0.01$ (the large points).

We see that for isothermal galaxies with $e = 0.5$, the cross section for magnified systems with undetectable extra images appears to be larger than the cross section for magnified

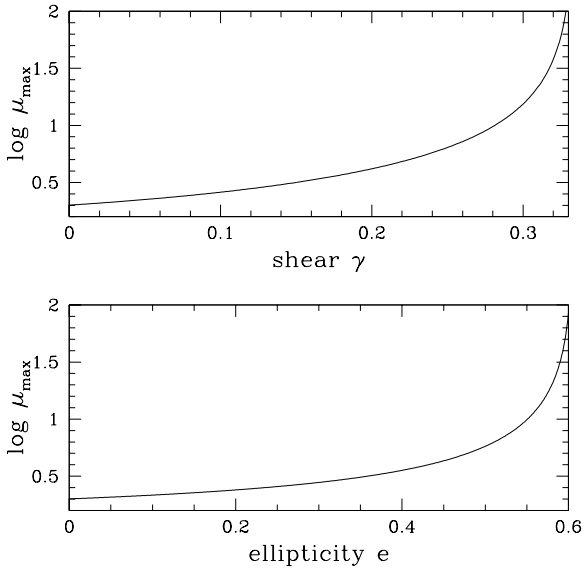

FIG. 2.— Maximum singly-imaged magnification for an isothermal sphere with shear (upper panel) and for an isothermal ellipsoid (lower panel). The maximum magnification becomes infinite at $\gamma = 1/3$ or $e = 0.606$ (see the Appendix for details).

singly-imaged systems. In the next two subsections we quantify this result carefully by computing the magnification cross sections for both cases.

3.2.1. *Singly-imaged magnification distributions*

For most isothermal lenses (unless the ellipticity or shear is large), there is a finite upper bound on the singly-imaged magnification. The bound is derived in the Appendix, and shown in Figure 2. While spherical models can never produce a singly-imaged magnification larger than $\mu_{\rm max} = 2$ (in the absence of microlensing; see Wyithe & Loeb 2002), non-spherical models can in principle produce much larger magnifications. However, the effect is not likely to be very dramatic in practice: for a typical shear $\gamma \sim 0.1$ or ellipticity $e \sim 0.3$, $\mu_{\rm max}$ is still less than 3.

The full magnification cross sections are shown in Figure 3 for various values of the parameters. Since all of the physical parameters — the lens galaxy mass and redshift, and the source redshift — are contained in the Einstein radius, the dimensionless cross section $A(\mu)/R_{\rm ein}^2$ depends only on ellipticity and shear so the parameter space we must study is small. Panels (a) and (b) show that shear and ellipticity increase not just $\mu_{\rm max}$ but the whole high-magnification tail. However, the cross section for high magnifications is small; even in models with large shear or ellipticity, the area in the source plane with $\mu > 10$ is less than 0.1% of the area with $\mu > 1.5$.

Shear and ellipticity are not mutually exclusive, so panel (c) shows what happens when we include both; we fix the amplitudes to typical values $\gamma = 0.1$ and $e = 0.3$ and vary the angle between them. The effects are largest when the shear and ellipticity are aligned, because they combine to increase the quadrupole moment of the lens potential; and the effects are smallest when they are orthogonal because their quadrupoles partially cancel. When averaged over angle, we expect the combination of shear and ellipticity to produce a modest increase in the area with modest magnifications.

3.2.2. *Multiply-imaged magnification distributions*

Sample multiply-imaged magnification distributions are shown in Figure 4. There are various unusual features that can be understood with the help of the corresponding source plane shown in Figure 1. Without imposing any single-detectable-image criterion (SDIC), the magnification cross section shows a kink at the minimum magnification for quads, and the high-magnification systems are dominated by quads (see, e.g., Blandford & Kochanek 1987; Schneider et al. 1992; Finch et al. 2002). SDICs remove the vast majority of quads, however, because the extra images in quads tend to be fairly bright. The only quad sources that survive the cut lie extremely close to the caustic, with image configurations dominated by a very bright and very close pair of images. In this example, when the flux ratio SDIC is $f < 0.1$ the magnification distribution is a smooth curve. However, when the flux ratio SDIC is $f < 0.01$ the distribution breaks up into two separate populations, with the low-magnification population lying just inside the radial caustic, while the high-magnification population lies just outside the cusps of the tangential caustic (see Figure 1). (The image separation SDIC is unimportant here because the Einstein radius is larger than the HST resolution.)

Having understood the general features, we can now examine how the multiply-imaged magnification distribution depends on ellipticity, as shown in Figure 5. In the absence of SDICs, ellipticity raises the high-magnification tail; for example, the cross section for $\mu > 10$ is increased by a factor of $\sim$2 for $e \gtrsim 0.5$. This case will apply to low-mass halos where the Einstein radius is small enough that all image separations are unresolvable. When the flux ratio SDIC is important (when the halo mass is large enough that the image separations would be resolved), ellipticity has a much more dramatic effect. In the spherical case there are no magnifications $\mu > 2/(1-f)$, where f is from the SDIC. Introducing ellipticity creates a population of high-magnification sources lying just outside the cusps of the tangential caustic. As e increases, that population grows and merges with the population of lower-magnification sources lying inside the radial caustic (as in Figure 4b). Finally, as the ellipticity grows to $e > 0.606$ the cusp of the tangential caustic pierces the radial caustic, so the high-magnification region just outside the cusp becomes associated with singly-imaged rather than multiply-imaged systems. This explains why the multiply-imaged cross section curve changes shape, but it is not very important in practice because such large ellipticities are rare.

The details clearly depend on the ellipticity and the SDIC, but the most important result is more general: the ordering of the curves in Figure 5. The dominant source of magnifications $\mu \gtrsim 5$ should be unresolvable small-separation lenses produced by low-mass halos, followed by systems with multiple images where the extra images are too faint to be detected. The contribution from true singly-imaged systems is generally not as important, except when the ellipticity is large ($e \gtrsim 0.6$), and even then the cross section is quite small.

Shear has similar effects on the magnification cross sections, because like ellipticity it increases the quadrupole moment of the lens potential and makes the tangential caustic larger. We do not show the cross sections for different shears, because the results appear very similar to those displayed in Figure 5.

3.3. *Averaging over Ellipticity and Shear*

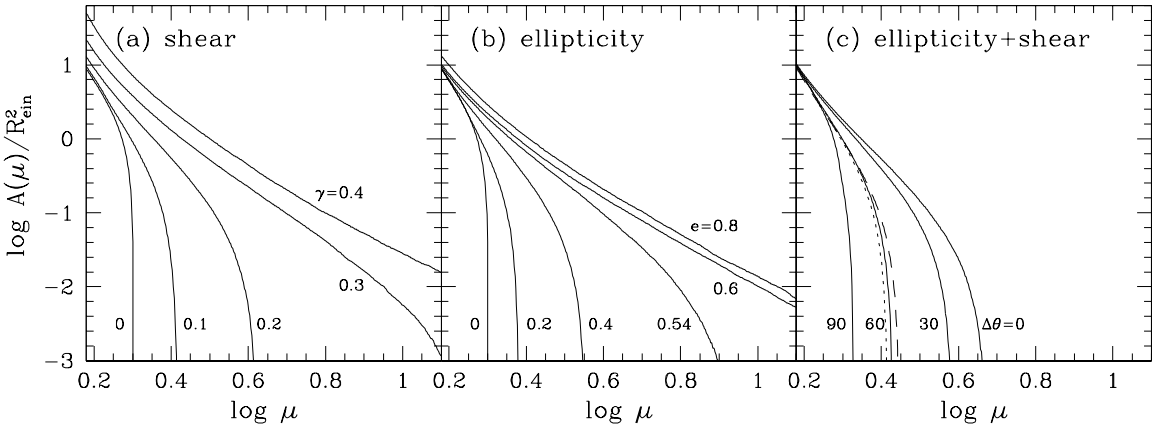

FIG. 3.— Singly-imaged magnification distributions for isothermal models. The area $A(\mu)$ where the magnification is greater than μ is expressed in units of $R^2_{\rm ein}$. (a) Effects of shear. (b) Effects of ellipticity. (c) Effects of ellipticity and shear together; the ellipticity and shear are fixed at $e = 0.3$ and $\gamma = 0.1$, and we vary the angle between them. For reference, the dashed curve shows a model with $e = 0.3$ and no shear, while the dotted curve shows a model with $\gamma = 0.1$ and no ellipticity.

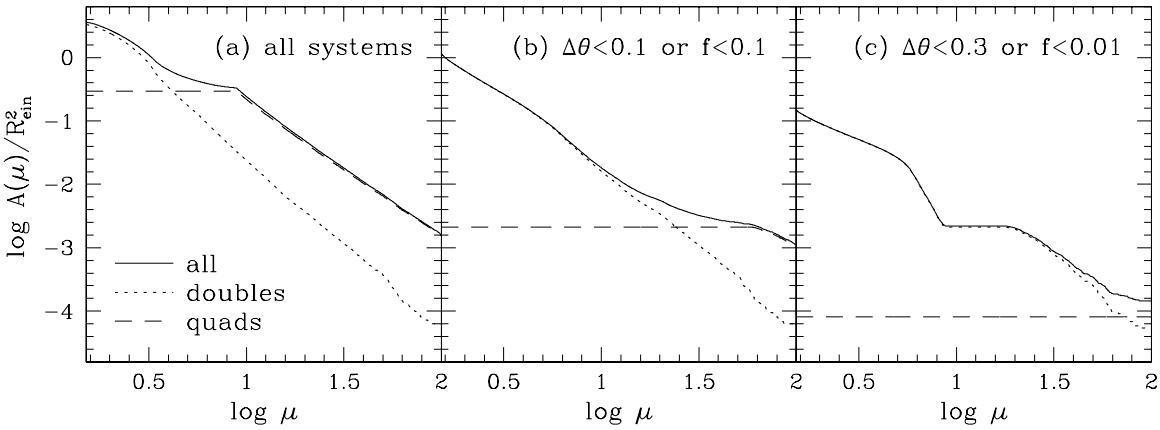

FIG. 4.— Multiply-imaged magnification distributions for an isothermal ellipsoid with ellipticity $e = 0.5$. The different line types denote different image configurations (doubles, quads, or all lenses). The different panels show different criteria for having only a single detectable image; panels (b) and (c) correspond to the detection limits in HST observations of the $z \approx 6$ SDSS quasars by Richards et al. (2004).

In order to obtain the overall probability distribution for the magnification, we next average over realistic distributions of ellipticity and shear. For the distribution of shear amplitudes, we use the model derived by Holder & Schechter (2003) for the environments of early-type galaxies in N-body and semi-analytic models of galaxy formation; they find a lognormal distribution with median $\gamma = 0.05$ and dispersion $\sigma_\gamma = 0.2$ dex. We use random shear directions. For the ellipticity distribution, we use data on the shapes of observed early-type galaxies.[7] Jørgensen, Franx, & Kjærgaard (1995) give ellipticities for 379 E and S0 galaxies in 11 clusters, including Coma. The distribution is broad, with mean $\bar{e} = 0.31$ and dispersion $\sigma_e = 0.18$. We average over more than 1000 random combinations of ellipticity and shear.

Figure 6 shows the resulting cross sections. Singly-imaged systems are important only for low magnifications ($\mu \lesssim 2$). If the Einstein radius is small and the lenses are unresolved, then multiply-imaged systems dominate at $\mu \gtrsim 1.8$; much of the relevant cross section comes from quads (as indicated by the difference between the solid and dashed curves). When the flux ratio SDIC applies, multiply-imaged systems dominate at $\mu \gtrsim 2.5$ for a SDIC of $f < 0.1$; for $\mu \lesssim 10$ most of this cross section comes from doubles, while for higher magnifications there is a significant contribution from quads. For a flux ratio SDIC $f < 0.01$, multiply-imaged systems dominate at $\mu \gtrsim 10$, and most of the cross section comes from doubles. The overall conclusion is that for isothermal halos, most large magnifications $\mu \gtrsim 10$ will correspond to multiply-imaged systems where the extra image are not detectable (either unresolved or faint).

We have explicitly examined ellipticity and shear, but early-type galaxies are also observed to have small octopole moments in their light distributions. We have repeated our analysis using the ellipticity and octopole distributions from the galaxy samples of Bender et al. (1989) and Saglia, Bender, & Dressler (1993), and confirmed that our results are not very sensitive to changes in the ellipticity distribution or to the addition of octopole terms.

[7] The data give the shape of the light distribution, while what we need is the shape of the mass distribution. The mass and light shapes may not be correlated on a case-by-case basis, but for our purposes it is sufficient to assume that their distributions are similar (see Rusin & Tegmark 2001).

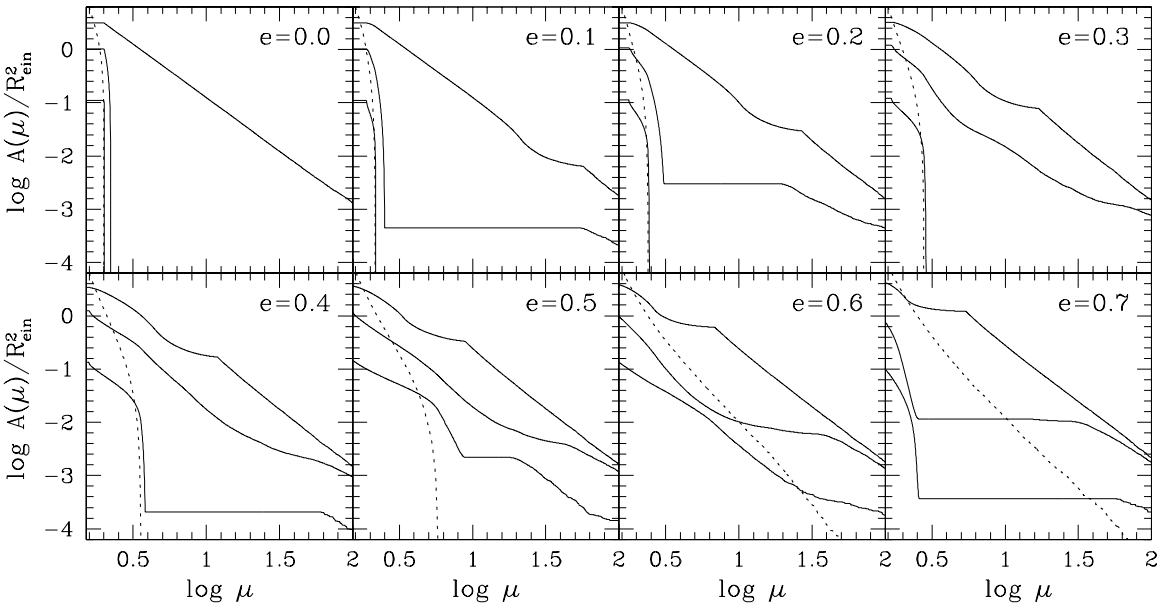

FIG. 5.— Effects of ellipticity on multiply-imaged magnification distributions for isothermal models. In each panel, the three solid curves show different criteria for having a single detectable image; the top curve shows all systems, the middle curve shows $\Delta\theta < 0.''1$ or $f < 0.1$, and the bottom curve shows $\Delta\theta < 0.''3$ or $f < 0.01$. For comparison, the dotted curve shows the appropriate singly-imaged magnification distribution (see Figure 3).

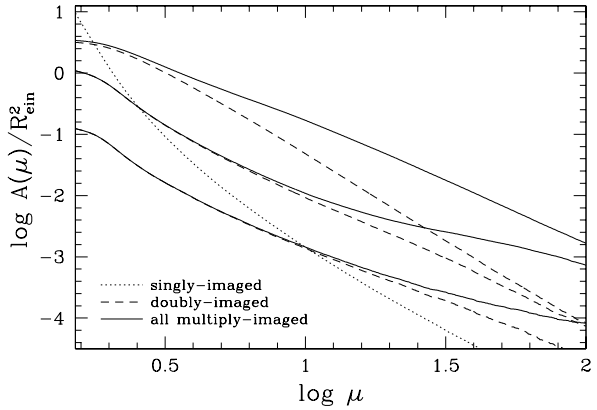

FIG. 6.— Magnification cross sections after averaging over ellipticity and shear. The dotted curve shows the singly-imaged cross section. The solid and dashed curves show the multiply-imaged cross sections. The top pair of curves includes all multiply-imaged systems (regardless of the number of detectable images). The middle pair corresponds to the following criteria for having a single detectable image: $\Delta\theta < 0.1 R_{\rm ein}$ or $f < 0.1$; while the bottom pair corresponds the criteria $\Delta\theta < 0.3 R_{\rm ein}$ or $f < 0.01$.

4. NFW HALOS

Another common and useful lens model is the Navarro-Frenk-White (NFW) profile, which describes halos produced in N-body simulations. The NFW profile is thought to describe systems that are dominated by dark matter at all radii: massive cluster halos, and perhaps low-mass dwarf halos as well. In this section we study the ability of NFW lenses to produce magnification without detectable multiple images.

4.1. *Definitions*

The NFW profile has the form

$$\rho(r) = \frac{\rho_s}{(r/r_s)(1+r/r_s)^2} \ , \qquad (8)$$

where r_s is a scale radius and ρ_s is a characteristic density. There has been debate about whether the inner density profile of simulated clusters really asymptotes to the $\rho \propto r^{-1}$ form (e.g., Navarro et al. 1997; Fukushige & Makino 1997; Moore et al. 1999; Jing & Suto 2000; Power et al. 2003; Fukushige et al. 2004), and whether such a density cusp is consistent with observed clusters (e.g., Tyson et al. 1998; Smith et al. 2001; Ettori et al. 2002; Kelson et al. 2002; Sand et al. 2002; Lewis et al. 2003; Sand et al. 2004). Our main need is for a model other than the isothermal ellipsoid that we can apply to massive clusters and low-mass dwarf halos. For this purpose the NFW model is standard and sufficient, and exploring a larger family of models (such as generalized NFW) is beyond the scope of this paper. Besides, with appropriate normalizations generalized NFW profiles lead to lens statistics that are not so sensitive to the inner profile slope (Keeton & Madau 2001).

The NFW profile has projected surface mass density (Bartelmann 1996)

$$\kappa(R) = 2\,\kappa_s\,\frac{1-F(R/r_s)}{(R/r_s)^2-1} \ , \qquad (9)$$

where $\kappa_s \equiv \rho_s r_s/\Sigma_{\rm crit}$ is a dimensionless lensing "strength" parameter, and the function $F(x)$ is:

$$F(x) = \begin{cases} (1-x^2)^{-1/2}\,\tanh^{-1}(1-x^2)^{1/2} & x<1 \\ 1 & x=1 \\ (x^2-1)^{-1/2}\,\tan^{-1}(x^2-1)^{1/2} & x>1 \end{cases} \qquad (10)$$

We obtain an elliptical NFW model by replacing $R \to (x^2 + y^2/q^2)^{1/2}$ in the surface mass density, where $q \le 1$ is the projected axis ratio, and the ellipticity is $e = 1-q$. The lensing properties of an elliptical NFW model can be computed with a set of 1-d numerical integrals (Schramm 1990; Keeton 2001b).[8]

[8] It is possible to obtain an analytic NFW model by putting the ellipti-

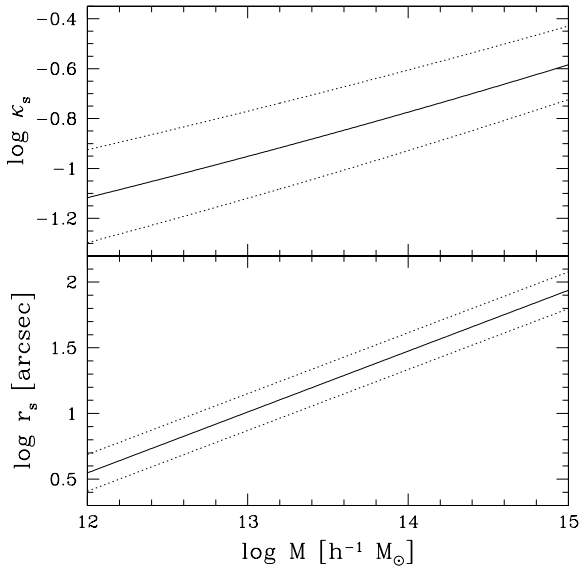

FIG. 7.— Sample lensing strength κ_s (upper panel) and halo scale radius r_s (lower panel) versus halo mass, for a lens at redshift $z_l = 1$ and source at redshift $z_s = 6$. The solid curves show results for halos with the median concentration, using the median $c(M)$ relation from Bullock et al. (2001); the dotted curves indicate the 1σ range due to the scatter in the M-c correlation, $\sigma_c = 0.14$ dex at fixed mass.

NFW profiles appear to form a two-parameter family specified by ρ_s and r_s, or equivalently by the virial mass M and a concentration parameter $c = r_{\rm vir}/r_s$. (The virial radius $r_{\rm vir}$ can be given as an explicit function of M and c.) In fact, the two parameters are correlated, and different models for median relation and scatter have been proposed (e.g., Navarro et al. 1997; Eke et al. 2001; Bullock et al. 2001; Jing & Suto 2002). For our purposes, the important result is that the scale length r_s and lensing strength κ_s are both correlated with the halo mass, as shown in Figure 7. In this section we can express cross sections in units of r_s^2 so we need not examine the r_s dependence explicitly; but we do need to examine the dependence on κ_s.

4.2. *Parameter Dependences for a Single Lens*

To begin to understand NFW lenses, in Figure 8 we show the source plane for a sample lens with strength $\kappa_s = 0.168$ (corresponding to a median $10^{14} M_\odot$ halo at $z_l = 1$, see Figure 7) and ellipticity $e = 0.1$. The caustics are small, and the region of multiply-imaged systems that satisfy reasonable single-detectable-image criteria (SDIC) is smaller still. The reason is that the image separations for massive halos are large, so the important SDICs involve the flux ratios. NFW halos generally produce large magnifications, and the range of magnification *ratios* is not very broad. As a result, the only sources that survive the SDICs lie very near the caustics, where one of the images has a very large magnification.

By contrast, there is quite a large region of the source plane where sources are singly-imaged but have large magnifications. Thus, for NFW halos it appears that singly-imaged systems will be more important than multiply-imaged systems for producing large magnifications with a single detectable image. In the next two subsections we quantify this result carefully.

4.2.1. *Singly-imaged magnification distributions*

Even spherical NFW lenses are complex systems where the lens equation is transcendental, so they must be studied numerically. Figure 9 shows the maximum singly-imaged magnification as a function of the strength κ_s. Spherical NFW halos can apparently produce large magnifications without multiple imaging, especially when the lensing strength (or halo mass) is small. It has been known that for multiple imaging at fixed splitting angle NFW lenses tend to produce smaller cross sections but larger magnifications than isothermal lenses (see Blandford & Kochanek 1987; Knudson et al. 2001). Now we see that the association between NFW lenses and high magnifications extends to single imaging as well.

The full magnification distributions are shown in Figure 10. Panel (a) shows that for spherical halos, increasing the strength κ_s decreases $\mu_{\rm max}$ but increases the overall cross section. Note that the figure shows the cross section in units of r_s^2; expressing the area in physical units like steradians would increase the distance between the curves, since the strength is correlated with r_s (see Figure 7).

Panels (b) and (c) in Figure 10 show that shear and ellipticity do not dramatically affect the magnification distributions for NFW halos. This stands in contrast to the case for isothermal halos. The difference is that the magnification distribution for spherical NFW halos already extends to high magnifications, so any increase due to ellipticity or shear is relatively more moderate. The departure from spherical symmetry does raise the tail to very high magnifications, but that effect is not very sensitive to the degree of asymmetry (shear or ellipticity). Interestingly, ellipticity appears to *lower* slightly the cross section for moderate magnifications. Finally, Figure 10d shows that allowing a combination of ellipticity and shear has little effect other than extending the high-μ tail of the distribution. While this is shown explicitly only for fixed $e = 0.3$ and $\gamma = 0.1$, we expect this generic feature to hold for other combinations.

4.2.2. *Multiply-imaged magnification distributions*

Figure 11 shows sample multiply-imaged magnification distributions for spherical NFW halos with different values of the lensing strength κ_s. Only the case with no regard for the number of detectable images is shown, because as we saw in Figure 8 the cross section for NFW lenses that satisfy the flux SDICs is extremely small. When the strength is low, the cumulative cross section $A(\mu)$ is flat out to $\mu > 100$, indicating that all magnifications are larger than 100; however, the cross section is very small. As κ_s increases, the point at which $A(\mu)$ begins to decline moves to the left, indicating that the minimum magnification decreases; and the cross section increases. For all but the most massive and concentrated halos, the multiply-imaged magnification cross section is considerably smaller than the singly-imaged cross section, except at the very highest (and rarest) magnifications.

A better way to compare the singly- and multiply-imaged cases is to take the ratio of the cross sections, as shown in Figure 12. Decreasing κ_s increases the ratio dramatically, so for moderate- to low-mass NFW halos the singly-imaged magnification cross section can be orders of magnitude larger than

cal symmetry in the potential rather than the density (e.g., Golse & Kneib 2002; Meneghetti, Bartelmann, & Moscardini 2003). However, N-body simulations suggest that it is the density rather than the potential that has ellipsoidal symmetry (or more generally, triaxiality; e.g., Jing & Suto 2002). We find that working with an elliptical density and using numerical integrals is not a major hindrance.

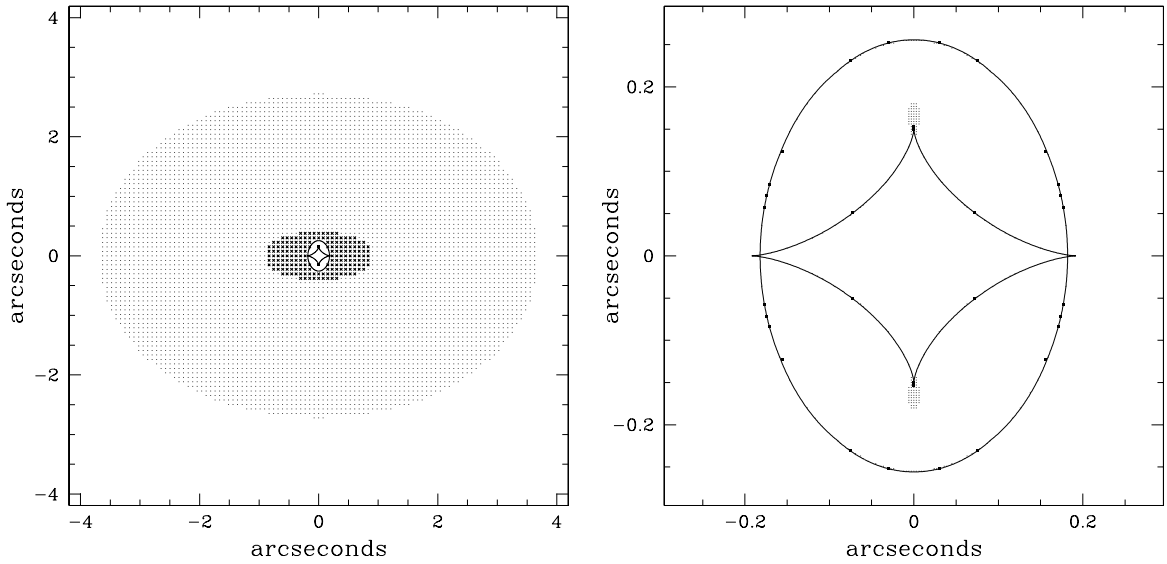

FIG. 8.— Source plane for an NFW halo with strength $\kappa_s = 0.168$, scale radius $r_s = 167\,h^{-1}$ kpc = 29.″8, and ellipticity $e = 0.1$. The curves show the caustics. The small (large) points outside the caustics indicate singly-imaged sources with magnification $\mu > 3$ ($\mu > 10$). The small points inside the caustic show multiply-imaged sources for which extra images are undetectable; the criteria for having only a single detectable image are an image separation $\Delta\theta < 0.''1$ or flux ratio $f < 0.1$ for the small points, and $\Delta\theta < 0.''3$ or $f < 0.01$ for the large points. The left panel shows a large region of the source plane, while the right panel shows a close-up of the multiply-imaged region.

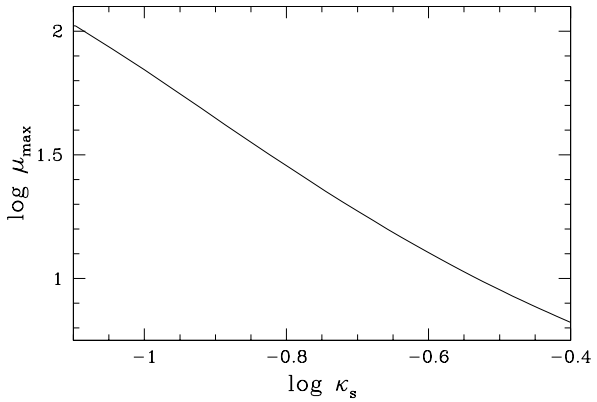

FIG. 9.— Maximum singly-imaged magnification versus lensing strength for spherical NFW lenses.

the multiply-imaged cross section. This quantifies the statement that for magnification by NFW halos, singly-imaged systems are vastly more important than multiply-imaged systems.

Figure 13 shows that ellipticity has little effect on the multiply-imaged magnification distribution. Large shears can in principle increase the cross section. However, it is not clear that massive NFW halos could experience such large shears. Shears of $\gamma \sim 0.2$–0.3 typically occur when the lens is a galaxy *within* a clusters, where the cluster serves as the environment that produces the shear. The filamentary structure typical around clusters represents a very different environment, for which the shear distribution is not well known. Fortunately, this uncertainty is not important for our results because shear and ellipticity have such modest effects. For simplicity, in the rest of the paper we consider only spherical halos when computing multiply-imaged magnification distributions for NFW halos.

5. A REALISTIC HALO POPULATION

Having understood two fiducial halo models, we now combine them into a realistic population of galaxies and clusters. We compute the overall probability for magnification with additional detectable images, and use it to evaluate the hypothesis that the four $z \approx 6$ SDSS quasars are highly amplified by lensing. After defining the model (§ 5.1), we present our general results (§ 5.2) and then apply them to the SDSS quasars (§ 5.3). We end with a discussion of some systematic effects in our analysis (§ 5.4).

5.1. *The Model*

The total probability distribution for μ comes from integrating the cross section over an appropriate halo population,

$$P(\mu; z_s) = \frac{1}{4\pi} \int dV \int dM \, \frac{dn}{dM} \, A(\mu; z_s, z_l, M) \,. \qquad (11)$$

The first integral is over the comoving volume between the observer and source. The second integral is over the comoving halo mass function dn/dM; we adopt the theoretical mass function from Sheth & Tormen (1999). Finally, $A(\mu)$ is the cross section computed above (expressed in steradians), which depends on the source redshift z_s, the lens redshift z_l, the lens halo mass M, and also on the lens model (isothermal or NFW). By using the appropriate cross section, we can compute the probability for singly-imaged or multiply-imaged magnifications by any of the halo populations we have considered.

Implicit in eqn. (11) is an average over appropriate ellipticity and shear distributions. For isothermal halos we use the results after averaging over ellipticity and shear, from § 3.3. Since the results for NFW halos are not very sensitive to ellipticity and shear, we simply use a fixed ellipticity $e = 0.1$ for the singly-imaged case (in order to pick up the

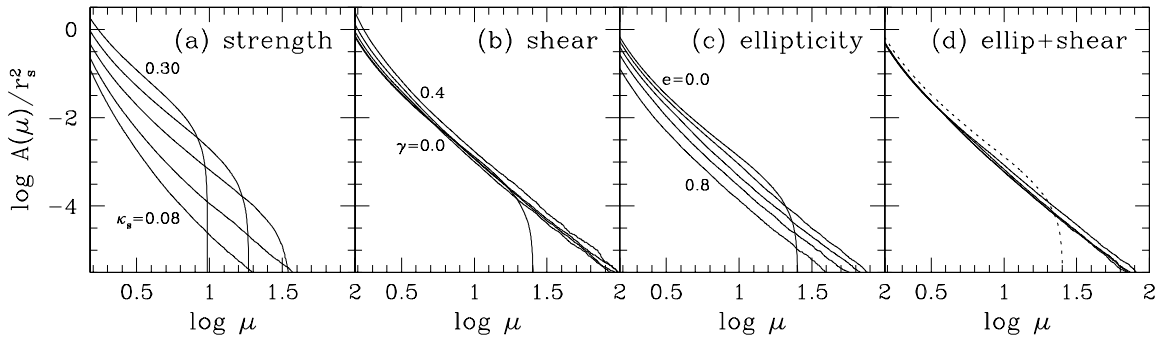

FIG. 10.— Singly-imaged magnification distributions for NFW models. The area $A(\mu)$ where the magnification is greater than μ is expressed in units of r_s^2 (not $R_{\rm ein}^2$). (a) Effects of the lensing strength κ_s; the curves show $\kappa_s = 0.08, 0.10, 0.14, 0.20, 0.30$ from bottom to top. (b) Effects of shear; the curves show $\gamma = 0, 0.1, 0.2, 0.3, 0.4$ from bottom to top. (c) Effects of ellipticity; the curves show $e = 0, 0.2, 0.4, 0.6, 0.8$ from top to bottom. (d) Effects of ellipticity and shear together; the curves show $\Delta\theta = 0, 30, 60, 90$ deg. The ellipticity and shear are fixed at $e = 0.3$ and $\gamma = 0.1$. For reference, the dotted curve shows a spherical model. In panels (b)-(d) the lensing strength is fixed at $\kappa_s = 0.168$ (the median value for a $10^{14}\,h^{-1}\,M_\odot$ halo in Figure 7).

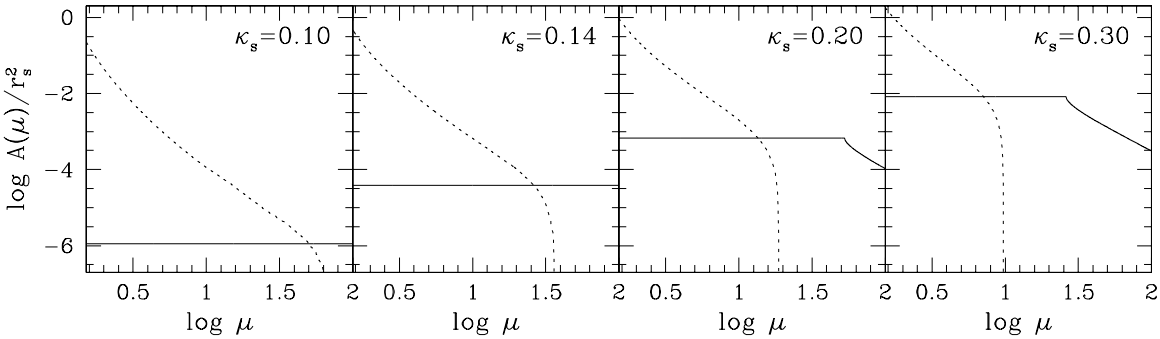

FIG. 11.— Magnification distributions for spherical NFW halos with different values of the lensing strength κ_s. The solid curves show multiply-imaged magnification distributions, regardless of the number of detectable images. For comparison, the dotted curves show the corresponding singly-imaged magnification distributions from Figure 10.

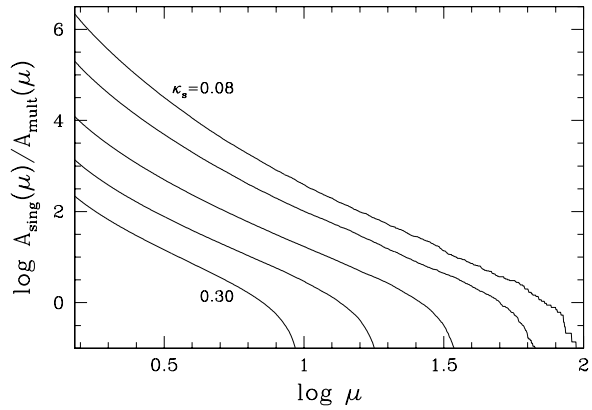

FIG. 12.— Ratio of singly-imaged and multiply-imaged magnification cross sections for NFW lenses. The curves correspond to $\kappa_s = 0.08, 0.10, 0.14, 0.20, 0.30$ from top to bottom.

high-magnification tail; see Figure 10), and we use spherical models for the multiply-imaged case.

We consider a model with at least two different halo populations. The most massive halos, corresponding to clusters and groups of galaxies, are treated as NFW halos; while halos corresponding to galaxies are modeled with isothermal profiles. In this increasingly standard model (Flores & Primack 1996; Keeton 1998; Porciani & Madau 2000; Kochanek & White 2001; Li & Ostriker 2002), the difference between clusters and galaxies is usually attributed to baryonic cooling: in massive halos the baryons have not had time to cool so the systems retain their initial NFW form; while in lower-mass halos the gas has cooled and condensed into the center of the system, and created a more concentrated total (baryons + dark matter) mass profile (e.g., Blumenthal et al. 1986; Kochanek & White 2001). Thus, the transition between clusters and galaxies is characterized by a mass scale $M_{\rm clus}$ such that halos with $M < M_{\rm clus}$ ($M > M_{\rm clus}$) have a cooling time shorter (longer) than the age of the universe and correspond to galaxies (clusters).

There may be a third population as well, namely low-mass "dwarf" halos with NFW profiles. Theoretical halo mass functions rise much more steeply than observed galaxy luminosity functions, leading to the speculation that there may be a substantial population of underluminous low-mass halos. Mechanisms such as feedback or reionization might have suppressed baryonic cooling and star formation in low-mass systems (e.g., Dekel & Silk 1986; Efstathiou 1992; Navarro & Steinmetz 1997; Thoul & Weinberg 1996; Bullock et al. 2000; Springel & Hernquist 2003), leading to halos that are dark and retain their initial NFW form. The apparent dearth of small-separation lens systems implies a transition from isothermal galaxies back to NFW dwarfs around

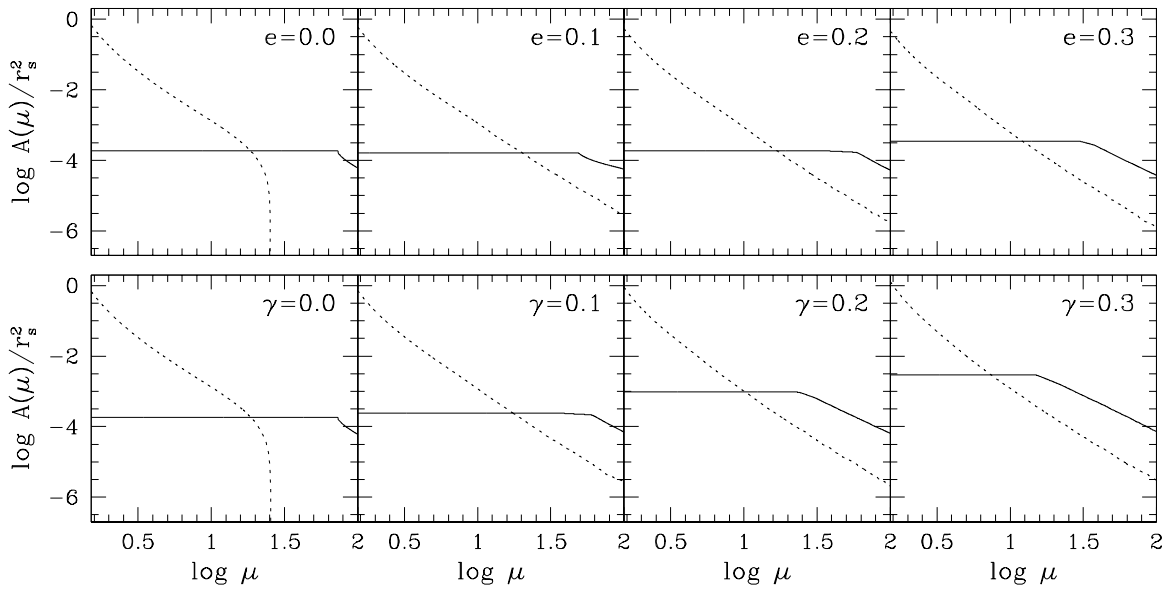

FIG. 13.— Magnification distributions for NFW halos with different ellipticities (upper panel) and shears (lower panel), with no regard for the number of detectable images. The lensing strength is fixed at $\kappa_s = 0.168$. For comparison, the dotted curves show the appropriate singly-imaged magnification distributions from Figure 10.

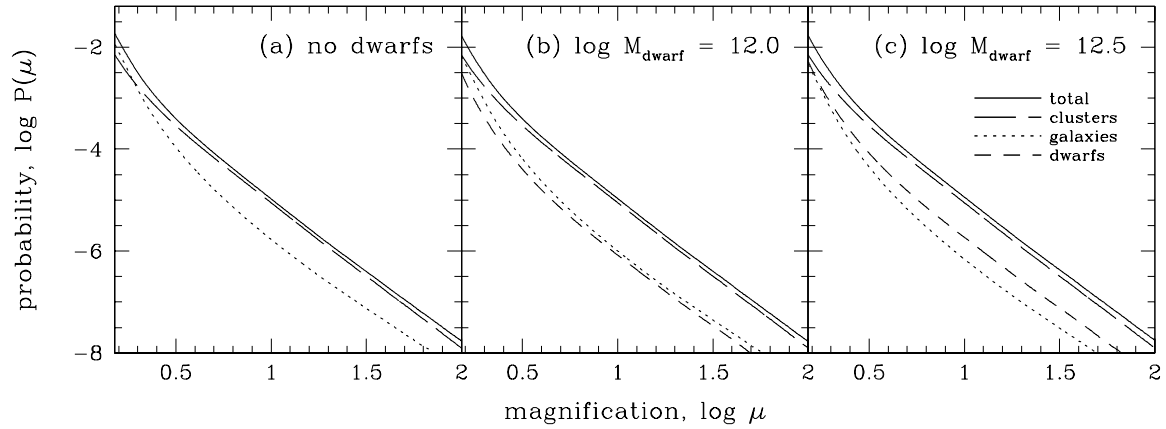

FIG. 14.— Net singly-imaged magnification probability distributions for sources at redshift $z_s = 6$. $P(\mu)$ is the cumulative probability of having a magnification greater than μ. The solid curves show the total probability, while the short-dashed, dotted, and long-dashed curves show the contributions from dwarf halos, normal galaxies, and clusters, respectively. The different panels correspond to different assumptions about the dwarf/galaxy transition (see text).

a mass of $M_{\rm dwarf} \sim 10^{12} M_\odot$ (Li & Ostriker 2003; Ma 2003; Kuhlen et al. 2004).

Following Ma (2003), we summarize the model by introducing a function $f_{\rm SIS}(M)$ that describes the fraction of halos of mass M that have isothermal profiles (and the rest are NFW). We use the function:

$$f_{\rm SIS}(M) = \begin{cases} 0 & M < M_{\rm dwarf} \\ 1 & M_{\rm dwarf} < M < M_{\rm clus} \\ \exp\left[-\frac{(\log M - \log M_{\rm clus})^2}{\sigma^2_{\rm clus}}\right] & M > M_{\rm clus} \end{cases} \quad (12)$$

To determine the parameter values, we follow Kuhlen et al. (2004) and fit the model to the observed image separation distribution from the Cosmic Lens All-Sky Survey (CLASS; Myers et al. 2003; Browne et al. 2003).[9] The formal best-fit model has $\sigma_{\rm clus} = 0.13$ and $\log M_{\rm clus} = 13.22$. However, there is a degeneracy between $\sigma_{\rm clus}$ and $M_{\rm clus}$ such that a model with a sharp transition ($\sigma_{\rm clus} = 0$) and $\log M_{\rm clus} = 13.38$ fits almost as well. We have verified that the two models give indistinguishable results, so we report results only for the model with a sharp transition. The cluster/galaxy transition mass inferred from lensing agrees well with estimates based on cooling arguments (e.g., Kochanek & White 2001). As for the galaxy/dwarf transition, current data lack any ability to determine whether it is smooth or sharp, so for simplicity we use only a sharp transition. The formal best-fit model has $\log M_{\rm dwarf} = 12.5$, although in fact only an upper limit on $M_{\rm dwarf}$ is reliable (see Kuhlen et al. 2004). This mass is too

[9] Our quantitative results differ slightly from the fiducial results of Kuhlen et al. (2004) because we now use the Sheth & Tormen (1999) mass function rather than that from Jenkins et al. (2001), and we use $\sigma_8 = 0.90$ rather than $\sigma_8 = 0.74$.

high to be explained by reionization feedback, so it might indicate either some other kind of feedback or some peculiarities in the data (perhaps unknown incompletenesses at small separations, or simply small-number statistics). We therefore consider several different values for $M_{\rm dwarf}$. We take the transition masses $M_{\rm clus}$ and $M_{\rm dwarf}$ to be independent of redshift. This assumption may seem objectionable, but we show below that the specific value of $M_{\rm clus}$ has little effect on our results, and we explicitly consider systematic uncertainties associated with $M_{\rm dwarf}$.

5.2. *Main Results*

Figure 14 shows the net singly-imaged magnification distribution, for our fiducial model. For sources at redshift $z_s = 6$, magnifications of $\mu \sim 1.6$ occur at the percent level, and the distribution drops quickly. The probabilities for $\mu > (2, 5, 10)$ are $(0.3\%, 9\times10^{-5}, 1.1\times10^{-5})$. In other words, significant singly-imaged magnifications are rare.

There are nevertheless several qualitative results that are interesting and instructive. First, for $\mu \gtrsim 1.8$ the singly-imaged magnification probability is dominated by clusters. This result seems at first glance to contradict Comerford et al. (2002), who found that massive NFW halos had negligible impact on the probability for lensing magnification, but the apparent discrepancy is easily explained. Comerford et al. considered lensing with undetected multiple imaging, while we are considering the complementary case where there is only a single image. NFW halos are much more efficient at producing highly magnified single images than multiple images (see Figure 12), which is why we find a much stronger effect. The important implication of this result is that if there is a significant singly-imaged magnification ($\mu \gtrsim 5$) then the lensing object is most likely a cluster, and ought to be relatively easy to detect. Conversely, lensing with small to moderate singly-imaged magnifications ($\mu \lesssim 2$) is dominated by galaxies. This is consistent with the claim by Shioya et al. (2002) that one of the $z \approx 6$ quasars is magnified by a factor $\mu \approx 2$ by a foreground galaxy, with no obvious sign of a cluster.

A second interesting feature of the singly-imaged magnification probability relates to the possible galaxy/dwarf transition at low masses. As discussed above, current lens data hint at the transition but do not constrain it well, so we consider three possible cases: (a) a model with no transition; (b) a model with the transition at $\log M_{\rm dwarf} = 12.0$; and (c) a model with the transition at $\log M_{\rm dwarf} = 12.5$, which perhaps seems high but is formally the best fit to current data (although it is not significantly better than the other models). Models (a) and (c) are extremes that bound the range of reasonable possibilities, and model (b) is a sample intermediate model. Not surprisingly, Figure 14 shows that moving the transition changes the relative contributions of galaxies and dwarf halos to the probability; if the transition occurs at $\log M_{\rm dwarf} \gtrsim 12.0$, dwarfs can conceivably contribute more of the probability than normal galaxies. But the important result is that changing $M_{\rm dwarf}$ affects the net probability by $<10\%$, since the singly-imaged case is dominated by clusters.

Figure 15 shows the multiply-imaged magnification probability, for different assumptions about the dwarf/galaxy transition and different single-detectable-image criteria (SDIC). In general, nearly all of the probability comes from galaxies. Clusters contribute $<10^{-5}$ of the probability if we consider all image configurations, and $<10^{-8}$ if we consider those with only a single detectable image; so we confirm the result from Comerford et al. (2002) that clusters are essentially negligible for the multiply-imaged magnification probability. NFW dwarfs halos, if present in the model, likewise have a negligible contribution to the probability (no more than $\sim10^{-7}$ even in the model with $\log M_{\rm dwarf} = 12.5$). The main effect of having dwarfs in the model is to reduce the number of halos that are isothermal galaxies, and hence to reduce the net multiply-imaged magnification probability. The reduction can be substantial when the SDICs are important.

TABLE 1.

Model	$F_{\rm sing}$	$F_{\rm mult}$	$F_{\rm tot}$
no dwarfs	0.049	0.241	0.290
$\log M_{\rm dwarf} = 11.0$	0.059	0.090	0.149
$\log M_{\rm dwarf} = 12.0$	0.080	0.014	0.094
$\log M_{\rm dwarf} = 12.5$	0.107	0.008	0.115

NOTE. — Fraction of lens systems magnified by $\mu > 10$ that lack extra images detectable by Richards et al. (2004). Columns 2-3 give the fractions that are singly-imaged and multiply-imaged, respectively, and Column 4 gives the total. Here we give results for a model with the dwarf/galaxy transition at $\log M_{\rm dwarf} = 11.0$, in addition to the three models discussed in the text.

Perhaps the most interesting result from Figure 15 is the effects of the SDICs. Consider the probability of a magnification $\mu > 10$, and suppose we have no knowledge of the presence or absence of additional images. Then we must use the multiply-imaged probability with no SDICs, and add the singly-imaged probability, which yields total probabilities of $(2.1, 1.4, 1.0)\times10^{-4}$ for models (a), (b), and (c) respectively. However, suppose like Richards et al. (2004) we can rule out the presence of extra images down to either $\Delta\theta = 0.''1$ and $f = 0.1$, or $\Delta\theta = 0.''3$ and $f = 0.01$. We should then use the lowest of the multiply-imaged curves in Figure 15, and again add the singly-imaged probability. A useful way to quantify the results is to give the fraction of systems magnified by $\mu > 10$ that do not have extra images detectable by Richards et al. (2004). This fraction is given by the *ratio* of the probability with SDICs to the probability without, or differences between the curves in Figure 15; the results are given in Table 1. For example, in the no-dwarf model, about 24% of highly magnified systems are multiply-imaged such that the extra images are undetectable, and another 5% are singly-imaged. In models with dwarfs, the fraction that are multiply-imaged without detectable extra images is much lower, so in total only 9–15% of highly magnified systems lack detectable extra images, and many of those are true singly-imaged systems lensed by clusters.

5.3. *Implications for the SDSS quasars*

So far we have only considered *a priori* lensing probabilities, i.e., the bare optical depth for producing certain magnifications. However, to compute the probability of finding a certain magnification in a real, flux-limited survey we would also have to fold in magnification bias to obtain *a posteriori* probabilities. Because the SDSS can probe only the steep, bright end of the quasar luminosity function at $z \approx 6$, magnification bias may be quite strong, but it is is extremely sensitive to the poorly-known LF shape. (In fact, the problem can be turned around so that lensing [or lack thereof] in the $z \approx 6$ quasar sample yields constrains on the LF slope; see Comerford et al. 2002 and Richards et al. 2004.) Rather than making detailed but highly LF-dependent predictions of the *a posteriori* probabilities, we turn attention to probability *ra-*

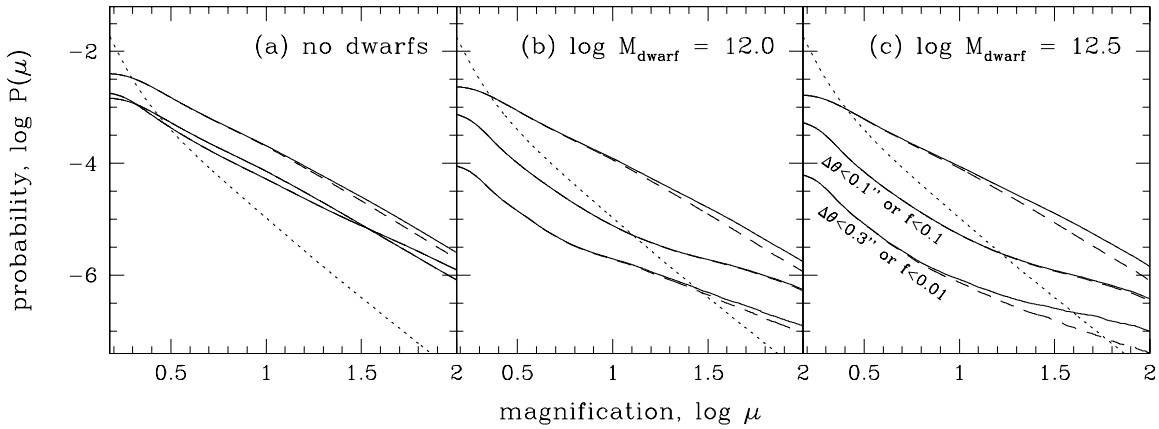

FIG. 15.— Net multiply-imaged magnification probability distributions for sources at redshift $z_s = 6$. In each panel, the upper solid curve shows the overall multiply-imaged probability (regardless of the number of detectable images), and the two other solid curves show the probability with different criteria for detecting only a single image (as indicated). The dashed curves show the contribution to each probability from galaxies alone (which is often indistinguishable from the total). The different panels correspond to different assumptions about the dwarf/galaxy transition. For comparison, the dotted curve shows the net singly-imaged magnification distribution from Figure 14.

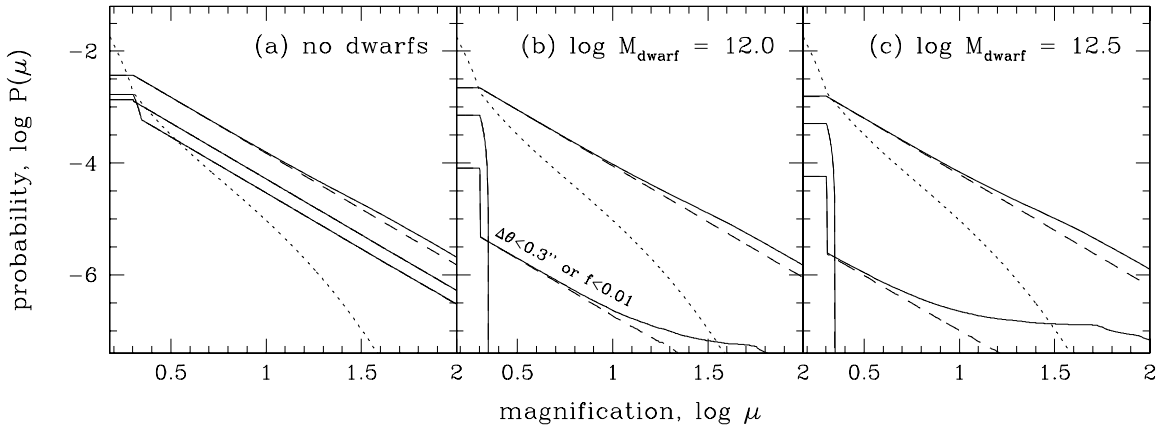

FIG. 16.— Similar to Figure 15, but for a model in which all halos are spherical and there is no shear.

tios and consider the following question: What is the ratio of the probability for $\mu > 10$ with observational SDICs, to the probability for $\mu > 10$ without SDICs? This is equivalent to the question: In a toy model with magnification bias so strong that *all* $z \approx 6$ quasars are magnified by a factor $\mu > 10$, what is the probability that one of the quasars would have no additional images detectable by Richards et al. (2004)?

In general, probability *ratios* should be the same for *a priori* and *a posteriori* probabilities, so Table 1 is exactly what we need. To summarize, if we are extremely optimistic about having strong magnification bias and about all low-mass halos having steep isothermal profiles, we can imagine that the probability of a $z \approx 6$ quasar being magnified by $\mu > 10$ without having additional images detectable by HST might be as high as 29%. If this is the case, we cannot rule out the possibility that one of the four $z \approx 6$ quasars observed by Richards et al. (2004) might actually be significantly magnified. However, even then the probability that *all four* are amplified would be $P = (0.29)^4 = 0.007$. The actual probability is almost certainly much lower, because magnification bias is probably not as strong as in the toy example, and because assuming that all low-mass halos have isothermal profiles probably overestimates the lensing optical depth. In other words, we can rule out at more than 99.3% confidence the hypothesis that all four $z \approx 6$ quasars are amplified by more than a factor of 10 — provided we can equate *a priori* and *a posteriori* probability ratios.

The only possible problem with equating the probability ratios is if the SDSS is somehow biased against high-redshift lensed quasars. Suppose, for the sake of argument, that there were a total of $4/0.29 = 14$ lensed and highly magnified $z \approx 6$ quasars in the SDSS, 10 of which have not been identified. Then having four quasars that are magnified but lack images detectable by Richards et al. (2004) would actually be consistent with the no-dwarf model. In our models with dwarfs, the total number of lensed quasars needed would be $\sim$25–45 (see Table 1). The key question is whether so many "missing" lensed high-redshift quasars could exist. The SDSS $z > 5.8$ quasar sample is selected on the basis of colors alone; the sample is basically *i*-dropouts, with some additional color criteria to reduce contaminants (Fan et al. 2000, 2001, 2003). There is no requirement that the objects ap-

pear point-like in SDSS images, and hence no bias against multiply-imaged systems. The only remaining problem is if light from a lens galaxy could change the composite colors of a lensed quasar system enough that the system would not be selected as an *i*-dropout. Lens galaxies associated with $z \approx 6$ lensed quasars would be expected to lie at redshifts $1 \lesssim z_l \lesssim 2$ (see Fig. 1 of Comerford et al. 2002), and so would probably be too faint to significantly change the colors (also see Wyithe & Loeb 2002). While it would be interesting to quantify this effect more carefully,[10] it seems unlikely that the SDSS high-redshift quasar sample is highly biased against multiply-imaged systems.

5.4. *Corollaries and Systematics*

We have obtained our main result, namely answering the question of whether it is likely that the $z \approx 6$ quasars are highly magnified, but there are several corollaries worth mentioning. First, so far in this section we have allowed the galaxies to have ellipticity and shear. (We have made certain assumptions about the ellipticity and shear for dwarf and cluster halos, but they are not so important; see § 5.1.) It is interesting to repeat the analysis with all halos assumed to be spherical, to see how much ellipticity and shear affect the results. Figure 16 shows the results. In the no-dwarf model, neglecting ellipticity and shear reduces the probability of multiple imaging with $\mu > 10$ by 30–50%. The same holds in models with dwarfs for the total multiple imaging probability (with no selection effects). However, in models with dwarfs where the SDICs apply, the reduction is at least a factor of 5 and often much larger. This result can be understood as follows. Most of the multiply-imaged magnification probability comes from the isothermal halos called "galaxies" in our model. If there are no dwarfs, then most of the probability comes from low-mass galaxies that produce image separations too small to be resolved; so the flux ratio SDIC is unimportant, and the probability is not dramatically sensitive to ellipticity (see the upper curves in Figure 5). By contrast, if low-mass halos are dwarfs (which have negligible cross sections), then much of the probability must come from galaxies that produce image separations larger than the resolution. In this case the flux ratio SDIC plays an important role; and in Figure 5 we saw that this dramatically reduces the cross section when the ellipticity is zero. The bottom line is that ellipticity and shear are a factor of $\sim$2 effect in no-dwarf models, but can be an order of magnitude effect in models with dwarfs.

The second point is that there are several additional systematic uncertainties that might be relevant. We have considered three effects that have the most impact on strong lens statistics (see Kuhlen et al. 2004): (i) changing the halo mass function from that of Sheth & Tormen (1999) to that of Jenkins et al. (2001); (ii) changing the scatter in the *M*-*c* correlation for NFW halos from 0.14 dex to 0.07 dex or 0.21 dex; and (iii) varying the location of the cluster/galaxy transition by $\Delta(\log M_{\rm clus}) = \pm 0.25$. We find that changing the mass function has the strongest effect, and even that is only a $\sim$10% change in the net magnification probability. In other words, our results appear to be robust to effects other than the question of whether low-mass halos are isothermal galaxies or NFW dwarfs.

Finally, our discussion has been geared toward sources at $z \approx 6$, but for completeness in Figure 17 we show the net *a priori* magnification probability as a function of source redshift. We use the no-dwarf model as a way to obtain an upper bound on the probability; for the multiply-imaged case we use the criteria $\Delta\theta < 0.''3$ or $f < 0.01$ for detecting only a single image, although from Figure 15a this choice is not so important. Reducing the redshift naturally reduces the probability, especially for $z_s \lesssim 3$. It affects the whole distribution in the same way, so our general conclusions appear not to be highly sensitive to the source redshift. Pushing quasar and galaxy samples beyond $z \approx 6$ will not significantly increase the probability for large lensing magnifications.

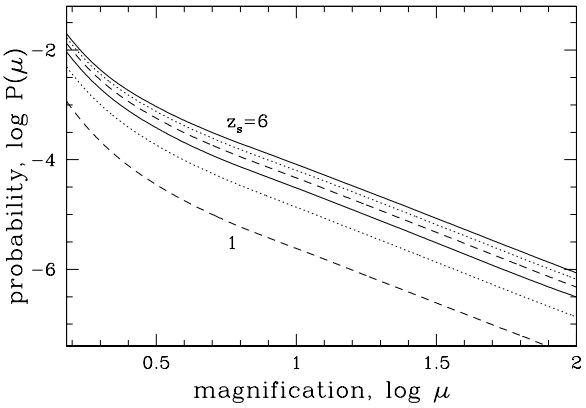

FIG. 17.— Total magnification probability distributions, including both the singly-imaged and multiply-imaged contributions, as a function of source redshift $z_s = 6, 5, 4, 3, 2, 1$ from top to bottom. Here we use the no-dwarf model to obtain the maximum possible probability.

6. CONCLUSIONS

The problem of lensing magnification without multiple detectable images has a rich phenomenology. First, there is the case of true singly-imaged systems. Isothermal halos are not very efficient at producing highly magnified single-image systems, but NFW halos are. Consequently, high singly-imaged magnifications are possible in principle, and they are mainly associated with massive ($\gtrsim 10^{13.5} M_\odot$) halos corresponding to clusters of galaxies. An important implication for observations is that, if there is no evidence for a cluster along the line of sight to a distant quasar, then it is unlikely that there is strong singly-imaged magnification.

The second case is when there are multiple images but the extra images are not detectable, either because the image splitting is too small to be resolved, or because the extra images are too faint. NFW halos are inefficient at producing multiple images, and when they do they rarely produce extreme flux ratios; therefore, clusters contribute negligibly to the multiply-imaged magnification probability. Instead, this case is dominated by galaxies and lower-mass systems ($\lesssim 10^{13} M_\odot$). The probability is very sensitive to the inner density profile of these halos. If all low-mass halos have steep isothermal profiles, then the probability is dominated by lens systems with image separations too small to be resolved by HST. However, if low-mass dwarf halos have NFW profiles (and hence small cross sections), then the overall probability is dominated by lens systems where the extra images are faint.

Our central quantitative result is that 9–29% of all lens systems with magnifications $\mu > 10$ lack additional detectable images. In a toy model where magnification bias is so strong that most or all $z \approx 6$ quasars are lensed, then we cannot rule

[10] An analysis that begins with the empirical correlation between image separation and lens galaxy luminosity (see the Appendix of Rusin et al. 2003a) would be reasonably straightforward.

out the hypothesis that one of the four quasars observed by Richards et al. (2004) is magnified despite lacking extra images. However, even in such an extreme model, the probability that *all four* are magnified by a factor of 10 would still be no more than 0.7%, and is probably much lower. The only way to evade this argument is if the SDSS high-redshift quasar sample is somehow biased against quasar lens systems with multiple bright images. That seems unlikely, although a detailed analysis of whether light from a lens galaxy could cause the *i*-dropout selection technique to miss a lens system is needed to answer this question definitively.

Incidentally, we can comment on the two different criteria used by Richards et al. (2004) to search for companion images to the $z \approx 6$ quasars. Richards et al. were able to rule out extra images down to a flux ratio $f = 0.01$ at image splittings greater than $0\farcs3$, or down to a less stringent flux ratio $f = 0.1$ for smaller image splittings down to $0\farcs1$. We find that for the no-dwarf model, the two criteria give similar probability results. By contrast, for models with dwarfs, the criteria with more stringent flux bounds provide stronger constraints on the lensing probabilities. In other words, for the purpose of determining whether distant quasars are magnified by lensing, it is more valuable to aim for more dynamic range than to push for resolution much better than $\sim 0\farcs3$.

To summarize, if the SDSS high-redshift quasar sample is not highly biased against multiply-imaged quasars, then it is quite improbable that all four quasars observed by Richards et al. (2004) are highly magnified. In that case, the quasars can be taken as good evidence for the presence of billion-$M_\odot$ black holes in the young universe. Explaining such black holes is a challenge for black hole growth models, whose solution may involve a need for super-Eddington accretion (Haiman 2004). In other words, in the case of high-redshift quasars, a lensing "null result" actually makes the objects even more interesting.

We thank Gordon Richards for helpful discussions about the SDSS high-redshift quasar sample. CRK is supported by NASA through Hubble Fellowship grant HST-HF-01141.01-A from the Space Telescope Science Institute, which is operated by the Association of Universities for Research in Astronomy, Inc., under NASA contract NAS5-26555. MQK is supported by NSF grant AST-0205738. ZH is supported by NSF grants AST-0307200 and AST-0307291.

APPENDIX

MAXIMUM SINGLY-IMAGED MAGNIFICATION FOR ISOTHERMAL LENSES

With isothermal lenses there are three simple cases in which the maximum singly-imaged magnification can be obtained analytically; the bounds were are shown in Figure 2 and are derived here. First, for a simple isothermal sphere the magnification of a singly-imaged source ($u > R_{\rm ein}$) is $\mu = 1 + R_{\rm ein}/u$, so the maximum magnification for singly-imaged sources is $\mu_{\rm max} = 2$. In fact, in this case the full singly-imaged magnification cross section can be derived analytically,

$$A(\mu) = \pi R_{\rm ein}^2 \left[\frac{1}{(\mu-1)^2} - 1 \right]. \qquad (1 < \mu < 2) \tag{A1}$$

Next consider an isothermal sphere with external shear. The magnification as a function of position is

$$\mu^{-1} = 1 - \gamma^2 - \frac{R_{\rm ein}}{R}\left(1 + \gamma\cos 2\theta\right). \tag{A2}$$

(We are now working in a coordinate system aligned with the shear, so $\theta_\gamma = 0$ in these coordinates.) The radial caustic is a circle with radius $R_{\rm ein}$. It maps to a curve in the image plane called the 1-2 transition locus, which marks the transition from single images to images that are part of a two-image system, and which can be written in polar coordinates as (Finch et al. 2002)

$$R_{1-2}(\theta) = 2R_{\rm ein}\left(\frac{1+\gamma\cos 2\theta}{1+2\gamma\cos 2\theta+\gamma^2}\right). \tag{A3}$$

For $\gamma < 1/3$ the radial caustic completely encloses the tangential caustic, so all sources outside the radial caustic and all images outside the 1-2 transition locus are singly-imaged. In this case, the maximum singly-imaged magnification occurs at $\theta = 0$ on the 1-2 transition locus,

$$\mu_{\rm max} = \frac{2}{(1-3\gamma)(1+\gamma)}. \qquad (\gamma < 1/3) \tag{A4}$$

For $\gamma > 1/3$ the tangential caustic pierces the radial caustic to form a naked cusp (e.g., Schneider et al. 1992; Finch et al. 2002). Sources just outside a naked cusp are singly-imaged but can have arbitrarily large magnifications, so $\mu_{\rm max} \to \infty$ in this case.

Finally consider an isothermal ellipsoid. The magnification as a function of position is

$$\mu^{-1} = 1 - \frac{b}{R}\left[\frac{2}{(1+q^2)-(1-q^2)\cos 2\theta}\right]^{1/2}. \tag{A5}$$

We cannot compute the full 1-2 transition locus, but we can compute where it intersects the x and y axes:

$$R_{1-2}(0) = \frac{2b}{\sqrt{1-q^2}}\tan^{-1}\left[\frac{\sqrt{1-q^2}}{q}\right] \tag{A6}$$

$$R_{1-2}(\pi/2) = \frac{2b}{\sqrt{1-q^2}}\tanh^{-1}\left[\sqrt{1-q^2}\right] \tag{A7}$$

The critical value of the axis ratio at which the tangential caustic pierces the radial caustic to form a naked cusp is found by solving

$$2\tan^{-1}\left[\frac{\sqrt{1-q^2}}{q}\right]-\frac{\sqrt{1-q^2}}{q}=0\,, \tag{A8}$$

whose solution is $q = 0.394$, or ellipticity $e = 0.606$. For $q < 0.394$, the presence of a naked cusp again causes $\mu_{\rm max} \to \infty$. For $q > 0.394$, the maximum singly-imaged magnification again occurs at $\theta = 0$ on the 1-2 transition locus and has the value

$$\mu_{\rm max}=\frac{qR_{1-2}(0)}{qR_{1-2}(0)-b}\,. \qquad (q>0.394) \tag{A9}$$

REFERENCES

Barkana, R., & Loeb, A. 2000, ApJ, 531, 613
Bartelmann, M. 1996, A&A, 313, 697
Bender, R., Surma, P., Döbereiner, S., Möllenhoff, C., & Madejski, R. 1989, A&A, 217, 35
Blandford, R. D., & Kochanek, C. S. 1987, ApJ, 321, 658
Blumenthal, G. R., Faber, S. M., Flores, R., & Primack, J. R. 1986, ApJ, 301, 27
Bouwens, R. J., et al. 2003, ApJ, 595, 589
Browne, I. W. A., et al. 2003, MNRAS, 341, 13
Bullock, J. S., Kravtsov, A. V., & Weinberg, D. H., 2000, ApJ, 539, 517
Bullock, J. S., Kolatt, T. S., Sigad, Y., Somerville, R. S., Kravtsov, A. V., Klypin, A. A., Primack, J. R., & Dekel, A. 2001, MNRAS, 321, 559
Comerford, J., Haiman, Z., & Schaye, J. 2002, ApJ, 580, 63
Dekel, A., & Silk, J. 1986, ApJ, 303, 39
Efstathiou, G. 1992, MNRAS, 256, 43P
Eke, V. R., Navarro, J. F., & Steinmetz, M. 2001, ApJ, 554, 114
Ettori, S., Fabian, A. C., Allen, S. W., & Johnstone, R. M. 2002, MNRAS, 331, 635
Fabbiano, G. 1989, ARA&A, 27, 87
Fan, X., et al. 2000, AJ, 120, 1167
Fan, X., et al. 2001, AJ, 122, 2833
Fan, X., et al. 2003, AJ, 125, 1649
Finch, T. K., Carlivati, L. P., Winn, J. N., & Schechter, P. L. 2002, ApJ, 577, 51
Fischer, P., Schade, D., & Barrientos, L. F. 1998, ApJ, 503, L127
Flores, R., & Primack, J. R., 1996, ApJ, 457, L5
Fukushige, T., & Makino, J. 1997, ApJ, 477, L9
Fukushige, T., Kawai, A., & Makino, J. 2004, ApJ, in press, astro-ph/0306203
Gerhard, O., Kronawitter, A., Saglia, R. P., & Bender, R. 2001, AJ, 121, 1936
Golse, G., & Kneib, J.-P. 2002, A&A, 390, 821
Haiman, Z. 2004, ApJ, submitted, astro-ph/0404196
Haiman, Z., & Cen, R. 2002, ApJ, 578, 702
Haiman, Z., & Loeb, A. 2001, ApJ, 552, 459
Holder, G., & Schechter, P. 2003, ApJ, 589, 688
Hu, E. M., Cowie, L. L., McMahon, R. G., Capak, P., Iwamuro, F., Kneib, J.-P., Maihara, T., & Motohara, K. 2002, ApJ, 568, L75
Huterer, D., Keeton, C. R., & Ma, C.-P. 2004, ApJ, submitted, astro-ph/0405040
Jenkins, A., et al. 2001, MNRAS, 321, 372
Jing, Y. P., & Suto, Y. 2000, ApJ, 529, L69
Jing, Y. P., & Suto, Y. 2002, ApJ, 574, 538
Jørgensen, I., Franx, M., & Kjærgaard, P. 1995, MNRAS, 273, 1097
Kassiola, A., & Kovner, I. 1993, ApJ, 417, 459
Keeton, C. R. 1998, Ph.D. thesis, Harvard Univ.
Keeton, C. R. 2001a, astro-ph/0102340
Keeton, C. R. 2001b, astro-ph/0102341
Keeton, C. R., & Kochanek, C. S. 1998, ApJ, 495, 157
Keeton, C. R., Kochanek, C. S., & Seljak, U. 1997, ApJ, 482, 604
Keeton, C. R., & Madau, P. 2001, ApJ, 549, L25
Kelson, D. D., Zabludoff, A. I., Williams, K. A., Trager, S. C., Mulchaey, J. S., & Bolte, M. 2002, ApJ, 576, 720
Kneib, J.-P., Cohen, J. G., & Hjorth, J. 2000, ApJ, 544, L35
Kneib, J.-P., Ellis, R. S., Santos, M. R., & Richard, J. 2004, ApJ, in press, astro-ph/0402319
Knudson, A., Ratnatunga, K. U., & Griffiths, R. E. 2001, AJ, 122, 103
Kochanek, C. S. 1998, in Science with the NGST, ed. E. P. Smith & A. Koratkar, ASP Conference Series vol. 133, p. 96
Kochanek, C. S., & White, M. 2001, ApJ, 559, 531
Koopmans, L. V. E., Treu, T., Fassnacht, C. D., Blandford, R. D., & Surpi, G. 2003, ApJ, 599, 70
Kormann, R., Schneider, P., & Bartelmann, M. 1994, A&A, 284, 285
Kuhlen, M., Keeton, C. R., & Madau, P. 2004, ApJ, 601, 104
Kundić, T., Cohen, J. G., Blandford, R. D., & Lubin, L. M. 1997a, AJ, 114, 507
Kundić, T., Hogg, D. W., Blandford, R. D., Cohen, J. G., Lubin, L. M., & Larkin, J. E. 1997b, AJ, 114, 2276
Lewis, A. D., Buote, D. A., & Stocke, J. T. 2003, ApJ, 586, 135
Li, L.-X., & Ostriker, J. P. 2002, ApJ, 566, 652
Li, L.-X., & Ostriker, J. P. 2003, ApJ, 595, 603
Ma, C.-P. 2003, ApJ, 584, L1
McKay, T. A., et al. 2002, ApJ, 571, L85
Meneghetti, M., Bartelmann, M., & Moscardini, L. 2003, MNRAS, 340, 105
Moore, B., Quinn, T., Governato, F., Stadel, J., & Lake, G. 1999, MNRAS, 310, 1147
Myers, S. T., et al. 2003, MNRAS, 341, 1
Navarro, J. F., Frenk, C. S., & White, S. D. M. 1997, ApJ, 490, 493
Navarro, J. F. & Steinmetz, M. 1997, ApJ, 478, 13
Ouchi, M., et al. 2003, ApJ, 582, 60
Pelló, R., Schaerer, D., Richards, J., Le Borgne, J.-F., & Kneib, J.-P. 2004, A&A, 416, L35
Pindor, B., et al. 2003, AJ, 125, 2325
Pirzkal, N., et al. 2004, ApJ, submitted, astro-ph/0403458
Porciani, C., & Madau, P. 2000, ApJ, 532, 679
Power, C., Navarro, J. F., Jenkins, A., Frenk, C. S., White, S. D. M., Springel, V., Stadel, J., & Quinn, T. 2002, MNRAS, 338, 14
Rhoads, J. E., Malhotra, S., Dey, A., Stern, D., Spinrad, H., & Jannuzi, B. T. 2000, ApJ, 545, L85
Rhoads, J. E., & Malhotra, S. 2001, ApJ, 563, L5
Richards, G. T., Strauss, M. A., Pindor, B., Haiman, Z., Eisenstein, D., Fan, X., & Schneider, D. P. 2004, AJ, 127, 1305
Rix, H.-W., de Zeeuw, P. T., Carollo, C. M., Cretton, N., & van der Marel, R. P. 1997, ApJ, 488, 702
Rusin, D., Kochanek, C. S., Falco, E. E., Keeton, C. R., McLeod, B. A., Impey, C. D., Lehár, J., Muñoz, J. A., Peng, C. Y., & Rix, H.-W. 2003, ApJ, 587, 143
Rusin, D., Kochanek, C. S., & Keeton, C. R. 2003b, ApJ, 595, 29
Rusin, D., & Tegmark, M. 2001, ApJ, 553, 709
Saglia, R. P., Bender, R., & Dressler, A. 1993, A&A, 279, 75
Sand, D. J., Treu, T., & Ellis, R. S. 2002, ApJ, 574, L129
Sand, D. J., Treu, T., Smith, G. P., & Ellis, R. S. 2004, ApJ, 604, 88
Schneider, P., Ehlers, J., & Falco, E. E. 1992, Gravitational Lenses (Berlin: Springer)
Schramm, T. 1990, A&A, 231, 19
Sheldon, E. S., et al. 2004, AJ, 127, 2544
Shioya, Y., et al. 2002, PASJ, 54, 975
Sheth, R. K., & Tormen, G. 1999, MNRAS, 308, 119
Smith, G. P., Kneib, J.-P., Ebeling, H., Czoske, O., & Smail, I. R. 2001, ApJ, 552, 493
Spergel, D. N., et al. 2003, ApJS, 148, 175
Springel, V., & Hernquist, L. 2003, MNRAS, 339, 289
Stanway, E. R., et al. 2004, ApJ, 604, L13
Steidel, C. C., Adelberger, K. L., Shapley, A. E., Pettini, M., Dickinson, M., & Giavalisco, M. 2003, ApJ, 592, 728
Thoul, A. A., & Weinberg, D. H. 1996, ApJ, 465, 608
Treu, T., & Koopmans, L. V. E. 2002, ApJ, 575, 87
Tyson, A., Kochanski, G., & dell'Antonio, I. 1998, ApJ, 498, L107
Willott, C. J., McLure, R. J., & Jarvis, M. J. 2003, ApJ, 587, L15
Witt, H. J., & Mao, S. 1997, MNRAS, 291, 211
Wyithe, S., & Loeb, A. 2002, ApJ, 577, 57
Zaritsky, D., & White, S. D. M. 1994, ApJ, 435, 599